DOI: https://doi.org/10.14311/TPFM.2023.014

MODEL ORDER REDUCTION FOR PARTICLE-LADEN FLOWS: SYSTEMS WITH ROTATIONS AND DISCRETE TRANSPORT OPERATORS

A. Kovárnová [1], M. Isoz [1, 2]

[1] **Department of Mathematics, Faculty of Chemical Engineering, University of Chemistry and Technology, Technická 5, Prague 166 28, Czech Republic**

[2] **Czech Academy of Sciences, Institute of Thermomechanics, Dolejškova 5, Prague 182 00, Czech Republic**

Abstract

In the present work, we concentrate on particle-laden flows as an example of industry-relevant transport-dominated systems. Our previously-developed framework for data-driven model order reduction (MOR) of such systems, the shifted proper orthogonal decomposition with interpolation via artificial neural networks, is further extended by improving the handling of general transport operators. First, even with intrusive MOR approaches, the underlying numerical solvers can provide only discrete realizations of transports linked to the movement of individual particles in the system. On the other hand, our MOR methodology requires continuous transport operators. Thus, the original framework was extended by the possibility to reconstruct continuous approximations of known discrete transports via another artificial neural network. Second, the treatment of rotation-comprising transports was significantly improved.

Keywords: Model order reduction, shifted POD, artificial neural networks, CFD-DEM, OpenFOAM.

1 Introduction

Particle-laden flows, i.e., flows comprising fluids and dispersed solid particles, are pervasive in scientific and engineering practice. However, these flows often exhibit complex coupling between the phases, which results in their high sensitivity to initial conditions and system parameters. Consequently, simulations of these flows tend to be complicated. The approaches to simulations of particle-laden flows can be divided into two main categories [1]. The first one, *Eulerian-Eulerian*, describes both the fluid and and the dispersed solid phase as two interpenetrating Eulerian continua and requires a solution of modified Navier-Stokes equations for those continua. This approach has relatively low computational costs and allows for simulations of large systems; however, it requires great number of empirical parameters in order to provide results of sufficient accuracy (e.g. [2]). In the second, *Eulerian-Lagrangian*, approach, only the fluid is represented as a Eulerian continuum and described via Navier-Stokes equations. In the solid phase, each particle is processed individually in its own Lagrangian coordinate system. Eulerian-Lagrangian methods generally require less parameters than Eulerian-Eulerian approaches. However, they pose greater demands on computational time [3].

These computational demands of Eulerian-Lagrangian methods for particle-laden flows can be problematic when industrial practice calls for optimization or system control based on these models. To solve this issue, various data-driven methods of model order reduction (MOR) have been developed, see e.g. [4]. In computational fluid mechanics, numerous MOR approaches rely on modal decomposition of the original system data [5]. One such approach is the proper orthogonal decomposition (POD) combined with the Galerkin projection to obtain a reduced order model (ROM) and discrete empirical interpolation method (DEIM) for treatment of system non-linearities [6]. However, any projection method requires the original system (full order model, FOM) to be described by a single set of partial differential equations, which is not the case of Eulerian-Lagrangian models for particle-laden flows. Therefore, another approach to ROM construction must be used.

Furthermore, the principle of mode-based methods and POD itself is to use the solution matrix $Y = (y_{ij}) = (y(x_i, t_j))$, $Y \in \mathbb{R}^{m\times n}$ and decompose it as [7]

$$Y \approx Y^\ell = \sum_{r=1}^{\ell} \psi_r \otimes \eta_r = \Psi^\ell H^\ell\,, \quad \Psi^\ell = [\psi_1, \ldots, \psi_\ell] \in \mathbb{R}^{m\times \ell}\,, \; H^\ell = [\eta_1, \ldots, \eta_n] \in \mathbb{R}^{\ell\times n}\,, \qquad (1)$$

where $\{\psi_r\}_{r=1}^{\ell}$ are stationary spatial modes, *toposes*, and $\{\eta_r\}_{r=1}^{\ell}$ are their time dependent amplitudes, *chronoses*. A single mode is then represented as a dyadic pair $\psi_r(x) \otimes \eta_r(t)$ and the whole matrix is approximated as a sum of the first ℓ modes, $\ell \ll n$.

However, particle-laden flows are usually transport-dominated and their behavior cannot be described by a superposition of just a few stationary modes, as all of their significant spatial structures are moving. Consequently, a great number of modes is needed for a sufficiently accurate approximation. Several approaches to solve this issue have been proposed, see e.g. [8, 9, 10, 11]. Usually, these methods use a time dependent shift to compensate for the transport. However, their application disallows for a straightforward application of projection-based MOR methods.

In the present work, we are interested in data-driven model order reduction of Eulerian-Lagrangian models of particle-laden flows. First, a low-rank approximation of the original data is constructed via the shifted orthogonal decomposition (sPOD), a method able to treat systems with multiple different transports by sorting the data into several co-moving frames of reference [8, 12]. Second, similarly to our previous work [13], the final reduced order model is prepared utilizing artificial neural networks (ANNs) instead of the standard Galerkin projection, which is not applicable.

The novelty of our work lies in extending the sPOD algorithm for treatment of general transport operators. First, while the theoretical treatment of operators comprising rotations remains as presented in [12], in practice, they require further modifications to the original method. Second, for the cases in which only discrete versions of the transport operators are known, another interpolating ANN was included in the final ROM.

The work is structured as follows. First, we outline the basic principles of shifted POD. Second, we discuss the treatment of systems with rotations. Next, we explain the final ROM structure, including ANN-based reconstruction of transport operators. In the result section, we present several examples of MOR of data generated by our in-house CFD-DEM code openHFDIB-DEM [14, 15].

2 Methods

Generally, MOR aims to reduce the computational costs of the system by reducing the number of its degrees of freedom (DoFs). Commonly, a mathematical model is defined by partial differential equations, which after spatial discretization via an arbitrary method (FVM, FEM, etc.) yield a system of ordinary differential equations that can be expressed in a form

$$\dot{y} = Ay + b(t, y)\,, \quad \forall t \in I\,,\, y(0) = y_0\,, \tag{2}$$

where y is the variable in question, Ay represents the linear part of the system and $b(t, y)$ its non-linearities. From now on, let us only consider this spatially discretized system and let us refer to it as to the full order model (FOM). The exact number of its DoFs depends on the specific problem and applied discretization, but in practice the number tends to go up to millions.

Our approach to MOR is an a-posteriori one, i.e., it is necessary to have available the solution, or snapshot, matrix $Y \in \mathbb{R}^{m\times n}$, where m is the number of spatial degrees of freedom and n is the number of saved times. For most a-posteriori methods, a low rank approximation of Y is computed first and then is used to generate a low-dimensional surrogate of (2).

A widely-used method for constructing a low rank approximation of Y is the proper orthogonal decomposition (POD), which technically corresponds to the truncated singular value decomposition (SVD) of the snapshot matrix, cf. (1) and

$$Y \approx Y^{\ell} = \Psi^{\ell} H^{\ell}, \quad H^{\ell} = \Sigma^{\ell} (X^{\ell})^{\mathrm{T}} \in \mathbb{R}^{\ell\times n}\,, \quad \Sigma^{\ell} = \operatorname{diag}(\sigma_1, \ldots, \sigma_{\ell})\,,\, X^{\ell} \in \mathbb{R}^{n\times\ell}\,. \tag{3}$$

The matrices Ψ^{ℓ} and X^{ℓ} originate from SVD and as such are composed of orthonormal column vectors. Hence, the relative importance of the modes is stored in their corresponding singular values in Σ, which are gradually decreasing. Therefore, based on the required approximation accuracy, it is possible to choose an $\ell \ll n$ and to construct the approximated matrix Y^{ℓ}, $\operatorname{rank}(Y^{\ell}) = \ell$ as a sum of the first ℓ modes.

Shifted proper orthogonal decomposition While POD is purely data-driven and no information on (2) is required for the construction of Y^{ℓ}, it approximates the matrix Y as a superposition of

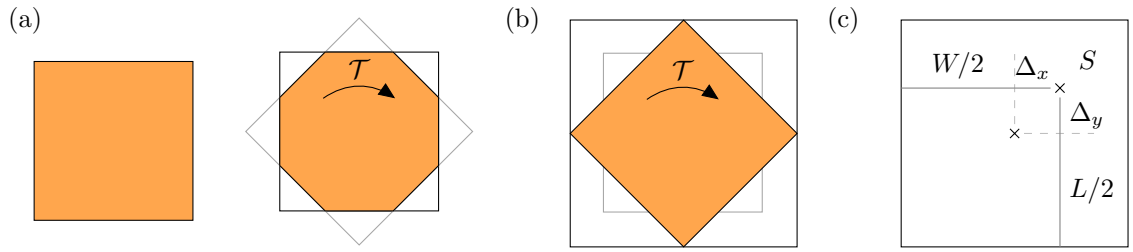

Figure 1: Data in the corners of the domain get lost during rotation (a) unless the domain is extended beforehand (b). The length of the extended domain is calculated based on the parameters in (c). S represents the axis of rotation.

ℓ *stationary* toposes. Thus, it is ineffective for systems with dominant transport, in which the position of their principal spatial structures changes in time. Consequently, a large number of modes is needed for an acceptably accurate approximation. However, the transport can be compensated with a time dependent shift $\mathcal{T}^{-\Delta^t}(f(t,x)) := f(t, x+\Delta^t)$. Such, *shifted* POD is significantly more effective for transport-dominated systems and a significantly smaller number of modes is sufficient. For illustration, see for example our previous contribution [13].

Taking into account that there might be multiple different transports in the system, the sought snapshot matrix approximation is given by

$$Y^\ell = (y^\ell(x_i,t_j)) = \sum_{k=1}^{N_\mathrm{f}} \mathcal{T}^{\Delta_k^t} \left(\sum_{r=1}^{\ell_k} \psi_r^k \otimes \eta_r^k \right) = \sum_{k=1}^{N_\mathrm{f}} \mathcal{T}^{\Delta_k^t} \left(\Psi_k^{\ell_k} H_k^{\ell_k} \right), \tag{4}$$

where N_f is the number of frames of reference.

The shifted proper orthogonal decomposition (sPOD) by Reiss et al. [8] used in this work builds on this idea and introduces an algorithm that is able to sort the data into multiple frames of reference. The exact algorithm is rigorously described in [12]; however, it is outside the scope of this work.

Implementation of shifts and treatment of rotation Our shifted POD variant is implemented in python and the shifts are realized via the module *ndimage*. Furthermore, only rectangular computational domains are taken into account in the present work. For the translation, the domain is assumed to be periodic and the shift is wrapped around, i.e., the information that comes out of the domain on one side can be stored on the other side.

The implementation of rotation is more complicated, as the data stored in the corners of the domain travels out and there is no obvious way as to where to store it, see Fig. 1a. Therefore, before the computation, the domain has to be extended and padded with zeros, see Fig. 1b. This approach increases the computational costs of SVD; however, no data is lost, and the added zeros do not affect the singular value decay in any way.

Considering only 2D cases and taking into account that the axis of rotation does not have to be equivalent with the center of the domain, the extended domain is square and its length is calculated as

$$L_\mathrm{new} = 2\sqrt{(W/2+\Delta_x)^2 + (L/2+\Delta_y)^2}, \tag{5}$$

where W and L is the width and the length of the original domain, respectively, and Δ_x and Δ_y the distance between the center of the domain and the axis of rotation along the x and y axis, respectively, see Fig. 1c. For the case of multiple frames with different values of Δ_x and Δ_y, the maximum value is used.

Projection methods and ANN interpolation as a data-driven alternative The general aim of MOR is not to merely construct Y^ℓ as an approximation of Y, but to obtain a low-dimensional surrogate for (2), i.e., to construct a mapping $\eta^\ell : I \to \mathbb{R}^\ell$, $\ell \ll m$. Usually, the surrogate is assumed to be in the form

$$\dot{\eta}^\ell = A^\ell \eta^\ell + f^\ell(t,\eta^\ell),\ \forall\, t \in (0,T], \quad \eta^\ell(0) = \eta_0^\ell, \tag{6}$$

where $A^\ell \in \mathbb{R}^{\ell\times\ell}$. The matrix A^ℓ and the system non-linearities $f^\ell(t, y^\ell)$ are commonly found via the Galerkin projection as

$$A^\ell = \left(\Psi^\ell\right)^{\mathrm{T}} A\Psi^\ell, \quad f^\ell(t, y^\ell) = (\Psi^\ell)^{\mathrm{T}} b(t, \Psi^\ell\eta^\ell), \quad y^\ell(0) = (\Psi^\ell)^{\mathrm{T}} y_0, \tag{7}$$

where $\Psi^\ell \in \mathbb{R}^{m\times\ell}$ is the projector obtained for example from POD (3).

The above outlined approach is not applicable for Y^ℓ obtained via the shifted POD (4). In particular, sPOD provides one projector for each frame of reference taken into account, $\Psi_k^{\ell_k}$, $k = 1, \ldots, N_\mathrm{f}$. Furthermore, let us recall that our full order model correponds to Eulerian-Lagrangian description of particle-laden flows. The flow is described in the Eulerian framework and for an incompressible Newtonian fluid, its governing equations are

$$\begin{aligned} \frac{\partial \boldsymbol{u}}{\partial t} + \nabla\cdot(\boldsymbol{u}\otimes\boldsymbol{u}) - \nabla\cdot(\nu\nabla\boldsymbol{u}) &= -\nabla\tilde{p} + \boldsymbol{s} \\ \nabla\cdot\boldsymbol{u} &= 0 \end{aligned} \tag{8}$$

where $\boldsymbol{u}$ is the velocity, $\tilde{p}$ kinematic pressure, ν the fluid viscosity and $\boldsymbol{s}$ is an immersed-boundary induced source term, for details see [14]. The particles $\{\mathcal{B}_i\}_{i=1}^{N_\mathcal{B}}$ are modeled within the Lagrangian framework, i.e., at any given time, each body is defined by its own system of six ordinary differential equations. For the particular body $\mathcal{B}_i$, the equations are

$$m_i \frac{\mathrm{d}^2\boldsymbol{x}_i}{\mathrm{d}t^2} = \sum_{j=1}^{N_f} \boldsymbol{f}_i^j\,, \quad I_i \frac{\mathrm{d}\boldsymbol{\omega}_i}{\mathrm{d}t} = \sum_{j=1}^{N_f} \boldsymbol{t}_i^j\,, \tag{9}$$

where m_i and $\boldsymbol{x}_i$ are the mass and center of $\mathcal{B}_i$, respectively. Furthermore, $\boldsymbol{\omega}_i$ is the body angular velocity and I_i is the matrix of its inertial moments. The sums on the right-hand sides of equations (9) represent, in order, all the forces $\boldsymbol{f}$ and torques $\boldsymbol{t}$ acting on $\mathcal{B}_i$.

While the system (8) can be converted into (2), the equations (9) cannot. The combination of restrictions imposed by replacing POD by sPOD and the ones enforced by the FOM structure (8) and (9) have led us to replace the standard projection methods by interpolation via artificial neural networks (ANN). The resulting framework is called sPODIANN (shifted Proper Orthogonal Decomposition with Interpolation via Artificial Neural Networks).

sPODIANN framework The general architecture of the sPODIANN framework was introduced in [13]. Its fundamental working principles are as follows. First, during the offline stage, sPOD is applied on the snapshot matrix, yielding $\Psi_k^{\ell_k}$ and $H_k^{\ell_k}$, $k = 1, \ldots, N_\mathrm{f}$. The times t and the time-dependent amplitudes $H_k^{\ell_k}$ for each frame are used as training data for an ANN, which produces the sought time-continuous surrogate $\tilde{\eta}^\ell(t)$. In the online stage, $\tilde{\eta}^\ell(t)$ is provided by the trained ANN. If the approximation of the full rank solution is required, it is obtained by substituting $\tilde{\eta}^\ell(t)$ into (4) and applying inverse transport operators $\mathcal{T}^{-\Delta_k^t}$, $k = 1, \ldots, N_\mathrm{f}$.

Note that this method is no longer *purely* data-driven – either the operators $\mathcal{T}^{\Delta_k^t}$, or at least their discrete versions $T^{\Delta_k^t}$, have to be known a-priori. If only the discrete versions are known, another ANN needs to be utilized to produce a time-continuous approximation $\tilde{\mathcal{T}}^{\Delta_k^t}$. Furthermore, the operators are required to be invertible up to an interpolation error and for the case of parametrized system, also continuous with respect to the parameters.

3 Examples

The applicability of the sPODIANN framework was already illustrated on three numerical examples in our previous contribution in [13]. Here, we show two other examples to demonstrate the two major improvements that have been presented in this work. The first one is a case with two discs freely falling through a domain, where only the discrete versions of the transport operators were known; therefore, another ANN was used to obtain their continuous approximation. The second example is a case with two discs circling through a domain on prescribed circular trajectories. This model was used to illustrate the framework extension for systems with rotation.

Both the systems were simulated using a CFD-DEM solver for particle-laden flows by Isoz et al. [14]. In this solver, the positions of the particles are prescribed via an indicator field λ, $\lambda = 0$ for cells inside the fluid, $\lambda = 1$ for cells inside the solid body and $\lambda \in (0; 1)$ for cells containing the solid-fluid boundary, with the exact value of λ depending on the percentage of the cell inside the solid.

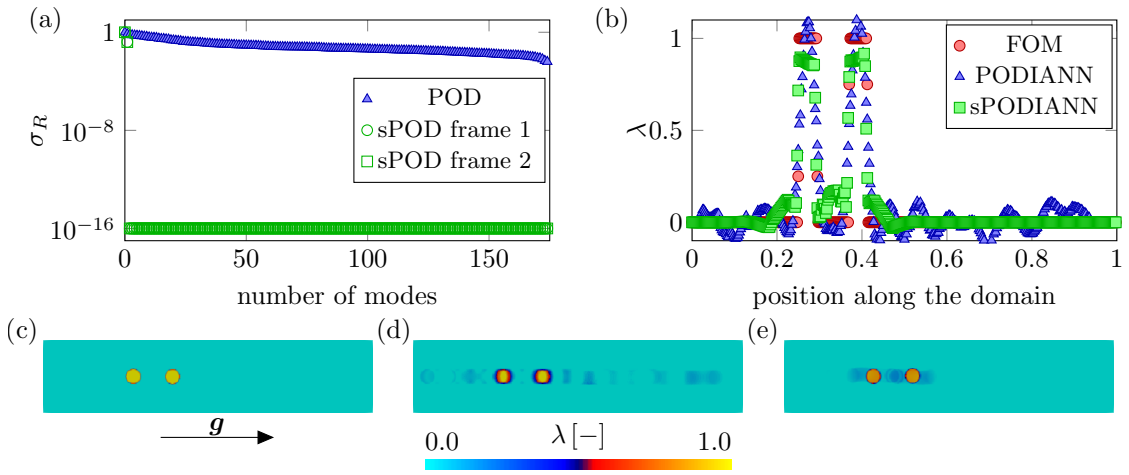

Figure 2: Two falling discs, λ (a) singular value decay for POD and both frames of sPOD, (b) slice of the λ field at $W/2$ in FOM, PODIANN and sPODIANN reconstruction, (c) – (e) qualitative view of the λ field at $t = 0.2$ for FOM, PODIANN and sPODIANN, respectively.

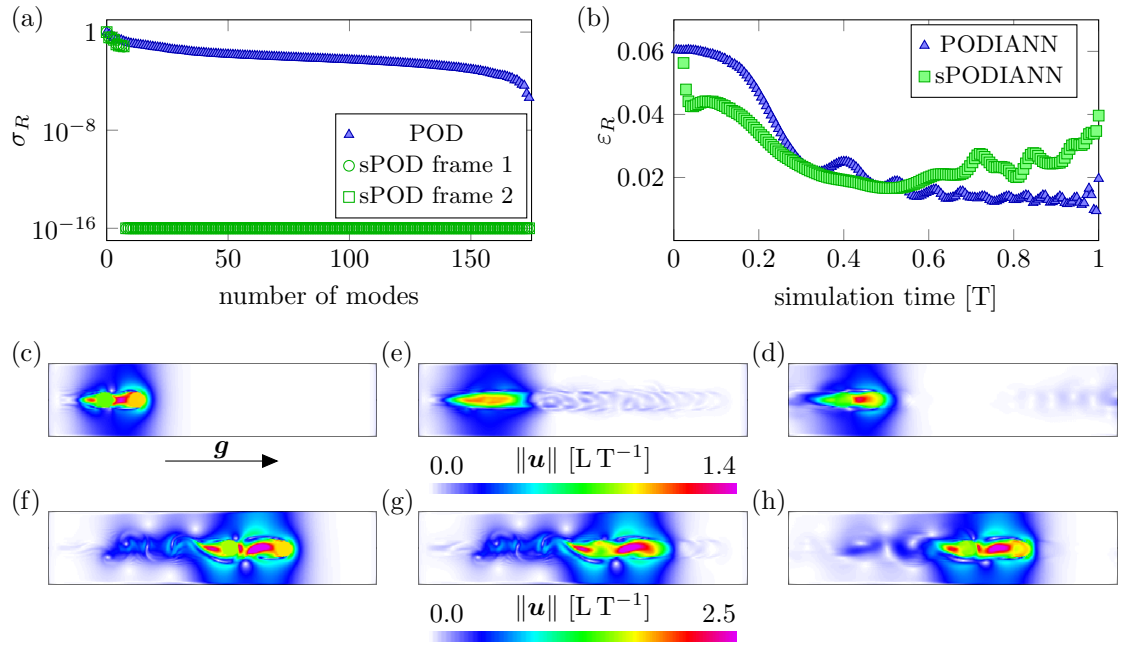

Figure 3: Two falling discs, velocity (a) singular value decay for POD and both frames of sPOD, (b) comparison of time evolution of the global relative error between ROM and FOM, (c) – (e) qualitative view of the velocity field at $t = 0.15$ for FOM, PODIANN and sPODIANN, respectively, (f) – (h) qualitative view of the velocity field at $t = 0.3$ for FOM, PODIANN and sPODIANN, respectively.

Falling spheres The first example is a system with two discs of different densities settling in a rectangular domain, $L = 0.46\mathrm{L}$, $W = 0.1\mathrm{L}$. The domain consists of 30 000 FVM cells and the FOM was prepared based on 175 snapshots. The domain is filled with fluid of density $\rho_\mathrm{f} = 1000\mathrm{ML}^{-3}$, while the densities of the discs are $\rho_1 = 2500\mathrm{ML}^{-3}$ and $\rho_2 = 3625\mathrm{ML}^{-3}$.

The movements of the discs are driven by gravity $\boldsymbol{g}$ and stem from the coupled fluid-solid interactions. As such, they are not known a-priori. However, the CFD-DEM solver provides us with information about the positions of the discs mass centers in discrete time steps, so the discrete versions of the shifts are of the form $T^{\Delta_k^t}$, $\Delta_k^t = \boldsymbol{r}_k(t) - \boldsymbol{r}_k(0)$. The continuous approximations $\tilde{\mathcal{T}}^{\Delta_k^t}$ are obtained using an ANN.

In Fig. 2 we present MOR of the λ field. As seen in Fig. 2a, the singular value decay for POD is extremely slow. On the other hand, sPOD is able to sort the data into two co-moving frames and in those it only needs two modes until it hits machine precision. Qualitatively, the POD-based reconstruction suffers from the so-called *staircase problem*, i.e., non-physical oscillations appearing instead of the traveling structures. See a slice through the λ field at $W/2$ in Fig. 2b, where oscillations were present even though 20 POD modes were used. Reconstruction using sPODIANN has no such deficiencies and produces satisfactory results using a single mode for each frame (2 modes in total). See the qualitative comparison of the λ fields shown in Fig. 2c, d and e.

The case of velocity field is more complicated. The velocity of the discs gradually increases, until at one point von Kármán vortices begin to shed. This qualitative change poses a problem for both POD and sPOD. The singular value decay is again faster for sPOD (see Fig. 3a); however, the global a-posteriori reconstruction error, calculated as

$$\varepsilon_R(t) = \frac{1}{m}\sum_{k=1}^{m} \frac{|\boldsymbol{u}_k(t) - \boldsymbol{u}_k^\ell(t)|}{\max_m\{|\boldsymbol{u}_k(t)|\} - \min_m\{|\boldsymbol{u}_k(t)|\}}, \tag{10}$$

where $\boldsymbol{u}_k$ is the FOM value of velocity in a cell k and $\boldsymbol{u}_k^\ell$ the ROM approximation, is comparable for both methods – between 1.5 and 6 %, see Fig. 3b. At the beginning, PODIANN produces non-physical oscillations, cf. Fig. 3c, d and e, but as the vortices begin to shed, the qualitative results of PODIANN and sPODIANN become quite similar to each other. Still, the vortices are more pronounced in the PODIANN reconstruction, see Fig. 3f, g and h.

Circling spheres The second case analysed is a model of two spheres moving through a square domain of $W = L = 0.2\mathrm{L}$ along prescribed circular trajectories, the first one defined by $S_1 =$

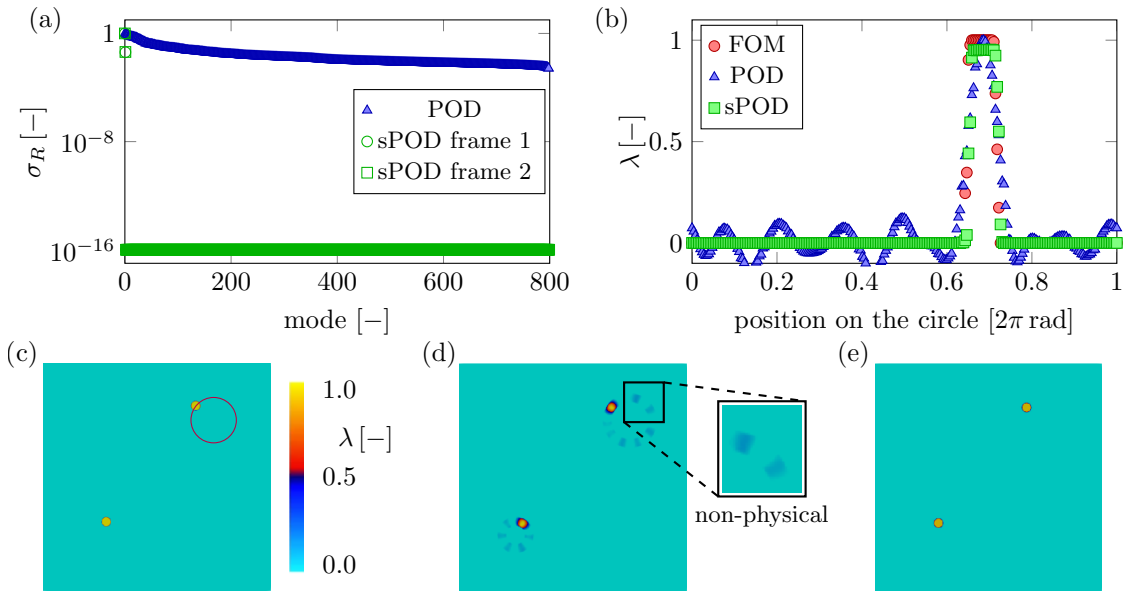

Figure 4: Two circling spheres, λ (a) singular value decay for POD and both sPOD frames, (b) slice of the λ field along the purple circle in (c) for FOM, PODIANN and sPODIANN reconstruction, (c) – (e) λ field at $t = 1.42$ for FOM, PODIANN and sPODIANN, respectively.

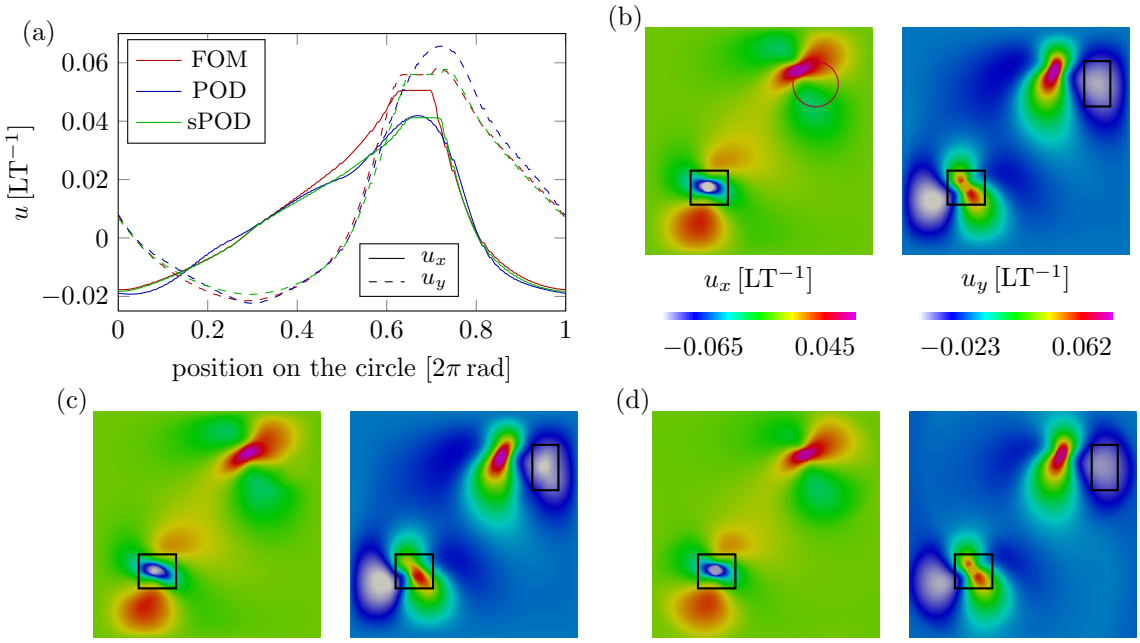

Figure 5: Two circling spheres, velocity (a) slice of the velocity field along the purple circle in (b) for FOM, PODIANN and sPODIANN reconstruction, (b) – (d) components of the velocity field at $t = 1.42$ for FOM, PODIANN and sPODIANN, respectively. Note the areas with the most distinct improvement of sPODIANN vs. PODIANN in black rectangles.

$(0.15, 0.15)$, $r_1 = 0.02\,\mathrm{L}$, $\omega_1 = 1.2\pi\,\mathrm{T}^{-1}$, the second one by $S_2 = (0.05, 0.05)$, $r_2 = 0.012\,\mathrm{m}$, $\omega_2 = 2\pi\,\mathrm{s}^{-1}$. Note that the linear velocity is identical for both spheres, as is the Reynolds number, $\mathrm{Re} = 0.6$. The domain consists of 230 400 FVM cells and the analysis was performed on 800 snapshots.

In Fig. 4, see an analysis of the λ field. The singular value decay is again significantly faster for sPOD. As in the case with falling discs, POD produces non-physical oscillations, this time plotted in Fig. 4b along the purple circle in Fig. 4c. For the qualitative comparison of FOM, PODIANN reconstruction using the first 24 modes and sPODIANN reconstruction using one mode for each frame, see Fig. 4c, d and e.

In Fig. 5, we present an analysis of the velocity field. The PODIANN reconstruction was prepared using the first 12 modes and the sPODIANN one using the first two modes for each frame (4 in total). Quantitative results are comparable, but sPOD produces better qualitative results, see a slice through velocity field in Fig. 5a made along along the circle in Fig. 5b. In Fig. 5b, c and d, see the qualitative view of the velocity components, where sPOD is able to better capture some of the finer structures highlighted by black rectangles.

4 Conclusion

In this contribution, we have extended our work on a framework combining shifted proper orthogonal decomposition with interpolation via artificial neural networks (sPODIANN). The shifted POD applies transport operators on the data and allows for siginificantly better dimensionality reduction of transport dominated systems, while the artificial neural networks (ANNs) make it possible to construct time-continuous reduced order models even for systems where the structure of the full order model is not suitable for standard MOR approaches, such as particle-laden flows. We have improved the framework and its treatment of general transport operators. By adding another interpolating ANN, we are now able to reduce even systems, where only the discrete analogues of the transport operators are known. In addition, the method is now able to treat systems with rotation more efficiently when the domain is extended beforehand. These improvements were illustrated on two CFD-DEM systems, where sPODIANN outperformed PODIANN (analogous method without shifts) in both cases.

Acknowledgment

The work was financially supported by the institutional support RVO:61388998 and by Grant project with No. TM04000048 of the Technology Agency of the Czech Republic.

References

[1] Marchisio, D. & Fox, R. *Multiphase reacting flows: modelling and simulation.* CISM International Centre for Mechanical Sciences. Springer Vienna: (2007). ISBN 9783211724637.

[2] G.D.R. Midi: On dense granular flows. *European Physical Journal E.* vol. 14: (2004). pp. 341–365.

[3] Azarpira, M., Zarrati, A. & Farrokhzad, P.: Comparison between the lagrangian and eulerian approach in simulation of free surface air-core vortices. *Water.* vol. 13: (03 2021). page 726. doi: 10.3390/w13050726.

[4] Fresca, S., Dede, L. & Manzoni, A.: A comprehensive deep learning-based approach to reduced order modeling of nonlinear time-dependent parametrized pdes. *J. Sci. Comput.* vol. 87: (2021). pp. 61–1–61–36. doi: 10.1007/s10915-021-01462-7.

[5] Taira, K., Hemati, M. S., Brunton, S. L., Sun, Y., Duraisamy, K., Bagheri, S., Dawson, S. T. M. & Yeh, C.-A.: Modal analysis of fluid flows: Applications and outlook. *AIAA J.* vol. 58: (2020). page 2737. doi: 10.2514/1.J058462.

[6] Chaturantabut, S. & Sorensen, D. C.: Nonlinear model reduction via discrete empirical interpolation. *SIAM J. Sci. Comp.* vol. 32: (2010). pp. 2737–2764. doi: 10.1137/090766498.

[7] Isoz, M.: POD-DEIM based model order reduction for speed-up of flow parametric studies. *Ocean Eng.* vol. 186: (2019). pp. 106083–1–106083–17. doi: 10.1016/j.oceaneng.2019.05.065.

[8] Reiss, J., Schulze, P., Sesterhenn, J. & Merhmann, V.: The shifted proper orthogonal decomposition: a mode decomposition for multiple transport phenomena. *SIAM J. Sci. Comput.* vol. 40: (2018). pp. A1322–A1344. doi: 10.1137/17M1140571.

[9] Rim, D., Peherstorfer, B. & Mandli, K. T.: Manifold Approximations via Transported Subspaces: Model reduction for transport-dominated problems. *arXiv e-prints.* (2019). page arXiv:1912.13024.

[10] Welper, G.: Interpolation of functions with parameter dependent jumps by transformed snapshots. *SIAM J. Sci. Comput.* vol. 39 no. 4: (2017). pp. A1225–A1250. doi: 10.1137/16M1059904.

[11] Krah, P. *Non-linear reduced order modeling for transport dominated fluid systems.* dissertation: Technical University Berlin: (2022).

[12] Reiss, J.: Optimization-based modal decomposition for systems with multiple transports. *SIAM J. Sci. Comput.* vol. 43: (2021). pp. A2079–A2101.

[13] Kovarnova, A., Krah, P., Isoz, M. & Reiss, J. Shifted proper orthogonal decomposition and artificial neural networks for time-continuous reduced order models of transport-dominated systems. In Simurda, D. & Bodnar, T., editors, *Proceedings of the conference Topical Problems of Fluid Mechanics*: pp. 111–118. IT CAS: Prague, Czech Republic: (2022).

[14] Isoz, M., Sourek, M. K., Studenik, O. & Koci, P.: Hybrid fictitious domain-immersed boundary solver coupled with discrete element method for simulations of flows laden with arbitrarily-shaped particles. *Computers & Fluids.* vol. 244: (2022). page 105538. ISSN 0045-7930. doi: https://doi.org/10.1016/j.compfluid.2022.105538.

[15] Sourek, M. & Isoz, M. Development of CFD solver for four-way coupled particle-laden flows. In Simurda, D. & Bodnar, T., editors, *Proceedings of the conference Topical Problems of Fluid Mechanics*: pp. 214–221. IT CAS: Prague, Czech Republic: (2020). doi: 10.14311/TPFM.2020.028.